THE JOURNAL OF BIOLOGICAL CHEMISTRY VOL. 283, NO. 51, pp. 35918–35928, December 19, 2008

Structural Determinants for Ca^{2+} and Phosphatidylinositol 4,5-Bisphosphate Binding by the C2A Domain of Rabphilin-3A*[S]

Received for publication, May 29, 2008, and in revised form, September 19, 2008 Published, JBC Papers in Press, October 21, 2008, DOI 10.1074/jbc.M804094200

Nicolas Coudevylle, Pierre Montaville, Andrei Leonov, Markus Zweckstetter[1], and Stefan Becker[2]

From the Department of NMR-based Structural Biology, Max-Planck-Institute for Biophysical Chemistry, Am Fassberg 11, 37077 Göttingen, Germany

Rabphilin-3A is a neuronal C2 domain tandem containing protein involved in vesicle trafficking. Both its C2 domains (C2A and C2B) are able to bind phosphatidylinositol 4,5-bisphosphate, a key player in the neurotransmitter release process. The rabphilin-3A C2A domain has previously been shown to bind inositol-1,4,5-trisphosphate (IP3; phosphatidylinositol 4,5-bisphosphate headgroup) in a Ca^{2+}-dependent manner with a relatively high affinity (50 μM) in the presence of saturating concentrations of Ca^{2+}. Moreover, IP3 and Ca^{2+} binding to the C2A domain mutually enhance each other. Here we present the Ca^{2+}-bound solution structure of the C2A domain. Structural comparison with the previously published Ca^{2+}-free crystal structure revealed that Ca^{2+} binding induces a conformational change of Ca^{2+} binding loop 3 (CBL3). Our IP3 binding studies as well as our IP3-C2A docking model show the active involvement of CBL3 in IP3 binding, suggesting that the conformational change on CBL3 upon Ca^{2+} binding enables the interaction with IP3 and vice versa, in line with a target-activated messenger affinity mechanism. Our data provide detailed structural insight into the functional properties of the rabphilin-3A C2A domain and reveal for the first time the structural determinants of a target-activated messenger affinity mechanism.

C2 domains are ubiquitous protein modules initially identified in protein kinase C (1). They all consist of ~130 residues (2) and share a common fold composed of two four-stranded β-sheets arranged in a compact β-sandwich and surrounded by variable loops and helices. C2 domain-containing proteins such as phospholipase C, cytosolic phospholipase A2, or protein kinase C are generally involved in signal transduction or membrane trafficking. The main function of the C2 domains in these proteins appears to be the targeting to biological membranes via their Ca^{2+}-dependent phospholipid binding properties (3). Primary lipid targets are phosphatidylcholine (for cytosolic phospholipase A2 (4)) and phosphatidylserine (for phospholipase Cδ (5), synaptotagmins (6), and protein kinase Cα (7)), the most abundant phospholipids in the inner membrane leaflet. Although not known to be classical phosphoinositide binding modules, some C2 domains have been shown to interact rather specifically with phosphoinositides (phospholipase C, protein kinase Cα), especially phosphatidylinositol 4,5-bisphosphate (PIP2)[3] (8). PIP2 represents less than 1% of the lipids in the plasma membrane and forms microdomains to regulate several key signaling events (9, 10). The interaction between the C2 domain of protein kinase Cα and PIP2 is essential for the proper subcellular localization of protein kinase Cα (11, 12). Several C2 domains of proteins involved in synaptic vesicle fusion have been described to bind PIP2, *e.g.* C2 domains of some synaptotagmins (6), CAPS-1 (13), and rabphilin-3A (14). The binding of the C2B domain of synaptotagmin 1 to PIP2 prelocalizes the protein to PIP2-enriched membranes (15). Recently a role for the CAPS-1 PIP2 interaction has been shown in the prefusion step of dense core vesicle fusion (13).

PIP2 is a key player in the different stages of the neurotransmitter release process. It is required for clathrin-mediated endocytosis (16) or for specific stages of exocytosis and synaptic vesicle trafficking (10). PIP2 recruits proteins to specific locations in the plasma membrane to modulate spatially localized events involved in membrane trafficking (17).

Rabphilin-3A was originally identified as a Rab3 effector in neuronal cells (18). It was found that the C-terminal C2 domain tandem (C2A and C2B) of this protein mediates interactions with β-adducin (19), calcium/calmodulin-dependent serine protein kinase (20), and annexin A4 (21). For the C2B domain a specific interaction with the tSNARE SNAP25 (25-kDa synaptosomal-associated protein) was identified (22). Recent results indicate that rabphilin-3A increases the number of releasable vesicles at the plasma membrane (22, 23) and enables the repriming of these vesicles after extensive evoked neurotransmitter release (23). The C-terminal C2 domains of rabphilin-3A are involved in the Ca^{2+}-dependent membrane targeting of rabphilin-3A (24), their primary target being the membrane phosphatidylserine. In addition, they have been described to bind

* This work was supported by the Max Planck Society. The costs of publication of this article were defrayed in part by the payment of page charges. This article must therefore be hereby marked "*advertisement*" in accordance with 18 U.S.C. Section 1734 solely to indicate this fact.

[S] The on-line version of this article (available at http://www.jbc.org) contains supplemental Figs. 1–4.

The atomic coordinates and structure factors (code 2K3H) have been deposited in the Protein Data Bank, Research Collaboratory for Structural Bioinformatics, Rutgers University, New Brunswick, NJ (http://www.rcsb.org/).

[1] Supported by Deutsche Forschungsgemeinschaft Heisenberg scholarship Z.W. 71/2-1 and 3-1).

[2] To whom correspondence should be addressed. Tel.: 49-551-201-2222; Fax: 49-551-201-2202; E-mail: sabe@nmr.mpibpc.mpg.de.

[3] The abbreviations used are: PIP2, phosphatidylinositol 4,5-bisphosphate; IP3, inositol-1,4,5-trisphosphate; CBR, Ca^{2+} binding region; CBL, Ca^{2+} binding loop; HSQC, heteronuclear single quantum correlation; NOESY, nuclear Overhauser effect (NOE) spectroscopy; r.m.s.d., root mean square deviation; RDC, residual dipolar coupling.

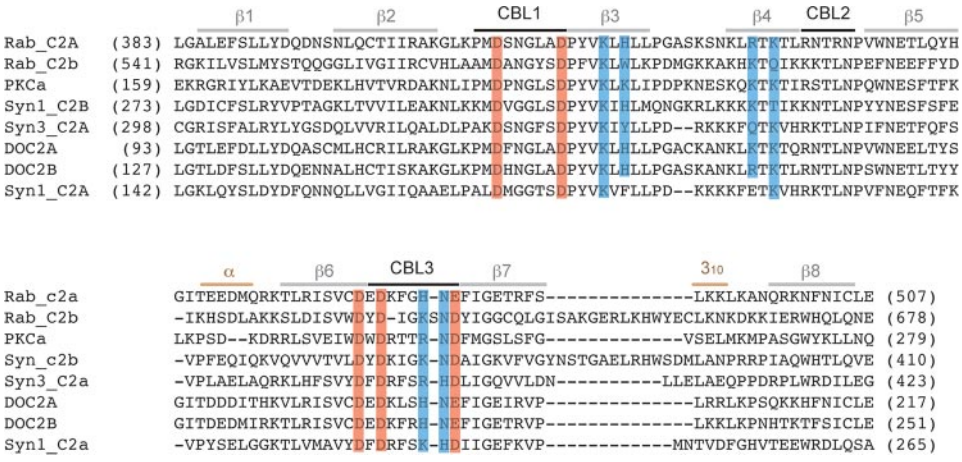

FIGURE 1. **Protein sequence alignment of several C2 domains from rat.** From *top to bottom*, C2A and C2B domains of rabphilin-3A (*Rab_C2A* and *Rab_C2B*, respectively), C2A domain of protein kinase Cα (*PKCa*), C2B domain of synaptotagmin-1 (*Syn_C2B*), C2A domain of synaptotagmin-3 (*Syn3_C2A*), C2 domains of DOC2A and DOC2B, C2A domain of synaptotagmin-1 (*Syn1_C2A*). Secondary structure elements shown on *top* correspond to the Ca^{2+}-free crystal structure of the rabphilin-3A C2A domain. Conserved residues involved in Ca^{2+} binding are highlighted in *red*, and conserved residues involved in PIP2 binding are highlighted in *blue*.

PIP2 *in vitro* (14), but so far no *in vivo* study has addressed the role of this interaction in rabphilin-3A function.

We have recently shown that rabphilin-3A C2 domains present well defined inositol 1,4,5-trisphosphate (IP3, *i.e.* PIP2 headgroup) binding sites in solution (25). However, the C2 tandem exhibits asymmetric behavior toward Ca^{2+} and PIP2 headgroup binding. The C2B domain binds Ca^{2+} with an affinity in the μM range and binds IP3 in a Ca^{2+}-independent manner with an affinity in the millimolar range (0.43 mM). Oppositely, the intrinsic Ca^{2+} binding affinity of the C2A domain is low (1.1 mM), and it binds IP3 in a Ca^{2+}-dependent manner with a relatively high affinity (50 μM) in presence of saturating concentration of Ca^{2+}. IP3 and Ca^{2+} binding to the C2A domain mutually enhance each other, in line with a target-activated messenger affinity mechanism where both the messenger and the target have to be simultaneously present to allow the protein to interact with them at physiological concentrations (26). The asymmetry of the rabphilin-3A C2 domains toward PIP2 headgroup binding may have functional implications; the C2A domain might be involved in the targeting of synaptic vesicle-bound rabphilin-3A to PIP2-enriched subdomains upon Ca^{2+} signaling. Subsequently, the C2B domain, once bound to the plasma membrane, might interact with the phosphoinositide during the docking step, potentially modulating its binding to SNAP25.

The functional plasticity found across the C2 domains is essential to convey specific functions to their harboring proteins. A more detailed structural characterization of specific C2 domain features should provide deeper insight into their functional properties. Within this line, the C2A domain crystal structure has been solved only in its Ca^{2+}-free state (27). Thus, the Ca^{2+} binding properties are not clarified yet. This domain binds Ca^{2+} cooperatively with a Hill coefficient of 2.24, suggesting that it binds two to three Ca^{2+} ions (25). But the exact binding mode remains unknown. Moreover, the Ca^{2+} binding region (CBR) of this domain exhibits several unusual features found only in a few other C2 domains (Fig. 1). In the Ca^{2+} binding loop 3 (CBL3), glutamic acid residues are found in position 482 (instead of a conserved Asp) and position 475 (instead of a conserved aromatic residue). The role and function of this non-canonical Ca^{2+} binding loop have been so far only poorly investigated. Finally, the structural features mediating the interrelation between Ca^{2+} and PIP2 headgroup binding remain mostly unknown. To address these structure-function aspects, we solved the solution structure of the rabphilin-3A C2A domain in its Ca^{2+}-bound form and investigated the structural determinants of its Ca^{2+} and IP3 binding properties.

EXPERIMENTAL PROCEDURES

Sample Preparation—The C2A domain (fragment 371–510) of rat rabphilin-3A was prepared as described previously (27, 28). ^{15}N- and ^{13}C,^{15}N-labeled samples were obtained by expressing the protein in minimal medium containing ^{15}N-labeled ammonium chloride and [^{13}C]glucose as sole nitrogen and carbon sources, respectively. All samples were concentrated up to 0.4 mM (for titration experiments) or 1 mM (for HSQC-NOESY experiments) in 20 mM sodium acetate, pH 5.0 (or 50 mM HEPES pH 7.0), 150 mM NaCl, and 1 mM dithiothreitol supplemented with 10% D_2O.

The C2A mutants (R432A, H480A, N481A, and N481D) were obtained using the QuikChange™ mutagenesis kit from Stratagene. The following primers were designed to introduce the mutations: R432A sense 5′-GTC CAA CAA GCT TGC TAC AAA GAC CCT GCG CAA CAC C-3′ and antisense 5′-GGT GTT GCG CAG GGT CTT TGT AGC AAG CTT GTT GGA C-3′; H480A sense 5′-GAG GAC AAG TTT GGC GCC AAT GAG TTC ATT GGT GAG ACC-3′ and antisense 5′-GGT CTC ACC AAT GAA CTC ATT GGC GCC AAA CTT GTC CTC-3′; N481A sense 5′-GAG GAC AAG TTT GGC CAC GCT GAG TTC ATT GGT GAG ACC-3′ and antisense 5′-GGT CTC ACC AAT GAA CTC AGC GTG GCC AAA CTT GTC CTC-3′; N481D sense 5′-GAG GAC AAG TTT GGC CAC GAT GAG TTC ATT GGT GAG ACC-3′ and antisense 5′-GGT CTC ACC AAT GAA CTC ATC GTG GCC AAA CTT GTC CTC-3′.

NMR Measurements—NMR experiments were carried out at 301 K on Bruker Avance spectrometers operating at 600, 800, or 900 MHz equipped with z-gradient cryoprobes. All spectra were processed using NMRPipe/NMRDraw (29) and analyzed with Sparky, Xeasy (30), and CARA (31). ^{1}H, ^{15}N, and ^{13}C assignment of the raphilin-3A C2A domain was taken from the Biological Magnetic Resonance Bank entry 6787 (32).

^{1}H,^{15}N HSQC-based titrations were performed using D-*myo*-inositol-1,4,5-trisphosphate (Calbiochem). Proton amide temperature coefficients were measured by performing ^{1}H,^{15}N HSQC experiments at different temperatures (279.2, 284.7, 289.2, 294.9, 299.6, and 305.4 K). Residual dipolar couplings

were measured on a partially aligned sample using bacteriophage Pf1 (Profos) at a concentration of 7 mg/ml at pH 6. One bond, $^{1}J_{^{1}H,^{15}N}$ and $^{1}D_{^{1}H,^{15}N}$, was measured on ^{1}H,^{15}N HSQC spectra acquired after the in-phase/anti-phase (IPAP) method (33). Interproton distances were derived from three-dimensional ^{13}C,$^{1}H/^{15}N$ HSQC-NOESY experiments performed with a mixing time of 120 ms.

Structure Calculations—Backbone φ and ψ dihedral restraints were derived from the program TALOS (34) using as input the ^{1}H, ^{13}C, and ^{15}N backbone chemical shifts. Only TALOS predictions with 10 matches agreeing were used as φ and ψ dihedral restraints. To each of them was attributed an average value with a minimal S.D. range of 10°. Dihedral restraints, ^{13}C,$^{1}H/^{15}N$ HSQC-NOESY spectra and ^{1}H, ^{13}C, ^{15}N chemical shifts were used as input for the ATNOS/CANDID package (35, 36) to generate a first ensemble of structures. This early ensemble was used to manually finalize the assignment of the ^{13}C,$^{1}H/^{15}N$ HSQC-NOESY spectra and led to a final set of about 1700 distance restraints. Dihedral angles and distance restraints were then used in the MD protocol of CYANA (37) to generate an ensemble of 100 structures of the rabphilin-3A C2A domain. Hydrogen-bond restraints were also added during this step, based on weak observed temperature coefficients (superior to $-5{\cdot}10^{-3}$ ppm·K^{-1}) (38) correlating with the secondary structure prediction.

The 50 structures with the lowest target function were selected for an RDC refinement protocol performed with Xplor-NIH (39) and the protein-2.0 force field. Ca^{2+} ions were added subsequently based on Ca^{2+} titration experiments and comparison with the canonical Ca^{2+} binding site of C2 domains. For each Ca^{2+}, six distance restraints were defined between the protein and the ion (Ca^{2+}-oxygen distances were restrained to 1.8–2.8 Å). The compatibility of the Ca^{2+} binding restraints with the force field parameters and the experimental restraints (dihedral angles, distance restraints, and RDCs) was carefully checked.

The 20 structures with the lowest energy were selected as the final ensemble of structures describing the rabphilin-3A C2A domain in solution. Experimental restraints and structural statistics are summarized in Table 1. The lowest energy structure from the final ensemble was considered as the most representative of the ensemble and was used for preparing figures and structure comparisons.

Fitting Procedure—To evaluate titration experiments of the labeled C2A domain with Ca^{2+} and IP3, the chemical shift deviations of significantly affected residues were plotted against the ligand concentration. A simultaneous fit was performed using Igor Pro (Wavemetrics Inc.) with the following equations. Equation 1 is a single binding site model (40),

$$\Delta\text{dppm} = B_{max}\frac{[Pt] + [Lt] + K_D - \sqrt{([Pt] + [Lt] + K_D)^2 - 4[Pt][Lt]}}{2[Pt]} \quad \text{(Eq. 1)}$$

where [Pt], [Lt], K_D and B_{max} are the total protein concentration, ligand concentration, dissociation constant, and the chemical shift deviation at saturation, respectively.

For the cooperative binding model, the total ligand concentration was used in the Hill equation to calculate the free ligand concentration,

$$\Delta\text{dppm} = B_{max}\frac{\left[[Lt] - \left[\frac{[Pt] + [Lt] + K_{Dapp} - \sqrt{([Pt] + [Lt] + K_{Dapp})^2 - 4[Pt][Lt]}}{2}\right]\right]^n}{K_{Dapp}{}^n + \left[[Lt] - \left[\frac{[Pt] + [Lt] + K_{Dapp} - \sqrt{([Pt] + [Lt] + K_{Dapp})^2 - 4[Pt][Lt]}}{2}\right]\right]^n} \quad \text{(Eq. 2)}$$

where [Pt], [Lt], K_{Dapp}, n, and B_{max} are the total protein concentration, ligand concentration, global dissociation constant, the Hill coefficient, and the chemical shift deviation at saturation, respectively.

Docking Models for the IP3-C2A Domain Complex—Models of the C2A-PIP2 complex were calculated using the docking program HADDOCK (high ambiguity-driven protein docking) (41) in combination with CNS (42) as described in our previous work (25). The five structures from the final ensemble with the lowest energy were used as starting coordinates for the C2A domain. Only solvent-accessible residues undergoing significant chemical shift perturbation ($\Delta\delta$ larger than 0.1 ppm) upon IP3 titration (performed at pH 5) were defined as active residues. More details about the docking protocol including a list of active residues and a full description of the docking consecutive stages are summarized in Table 2.

The 50 structures obtained after water refinement were analyzed and ranked according to their HADDOCK score (Table 2). The three best models were selected as the final representative ensemble of the complex structure.

RESULTS

Structural Statistics and Overall Structure of the Ca^{2+}-bound C2A Domain of Rabphilin-3A—The solution structure of the Ca^{2+}-bound C2A domain of rabphilin-3A was solved with the aim of investigating its IP3 binding properties including the way they are modulated by Ca^{2+}. Because amide resonances of residues from CBL3 were broadened below detection level at pH 7, all spectra were acquired at pH 5. The N-terminal portion of the C2A domain fragment (residues 371–383) was not included in the structure calculation as it has been observed to be highly dynamic. Indeed, only few sequential NOE effects were observed for this segment (as also revealed by the very narrow line-widths of ^{1}H,^{15}N HSQC cross-peaks for these residues).

The 20 final structures of the Ca^{2+}-bound C2A domain of rabphilin-3A at pH 5 exhibit an atomic root mean square distribution about the mean coordinate positions of 0.38 ± 0.11 Å for the backbone atoms and 1.11 ± 0.14 Å for all heavy atoms, excluding the residues from CBL1 and CBL3, which are slightly less well defined (Fig. 2*A*). The structure ensemble fits the experimental restraints with no interproton distance and torsion angle violations greater than 0.2 Å and 10°, respectively. All of the backbone torsion angles of the non-glycine residues fall in the allowed regions of the Ramachandran plot (Table 1).

The overall structure is composed by two four-stranded β-sheets arranged in a compact β-sandwich (corresponding to the type I topology described for the C2 domains) and sur-

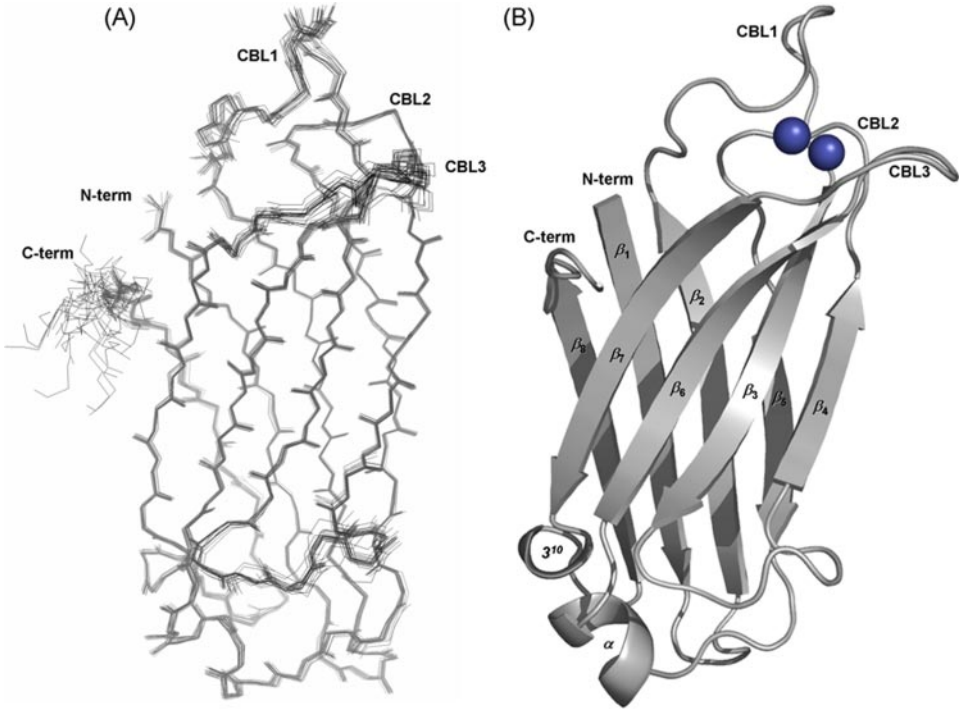

FIGURE 2. **Overall solution structure of the Ca^{2+}-bound rabphilin-3A C2A domain.** *A*, backbone superimposition of the final set of 20 structures for the C2A domain. *B*, representative ribbon model of the C2A domain. Ca^{2+} ions are depicted as *blue spheres*.

TABLE 1
NMR and refinement statistics for rabphilin-3A C2A domain

NMR geometric restraints	
Total distance restraints	1803
Intra-residue	705
Inter-residue	1098
Sequential ($\|i-j\| = 1$)	527
Medium-range ($\|i-j\| \leq 4$)	151
Long-range ($\|i-j\| \geq 5$)	420
Hydrogen bonds[a]	57
Ca^{2+}-protein restraints[b]	12
Total dihedral restraints	170
φ	84
ψ	86
Total $^1D_{1H-15N}$ residual dipolar couplings	90
Structure statistics	
Violations (r.m.s.d. and S.D.)	
Distance restraints	0.0104 ± 0.0006
Dihedral restraints	0.81 ± 0.02
$^1D_{1H-15N}$ RDC	0.72 ± 0.01
Deviation from idealized geometry	
Bond lengths (Å)	0.00281 ± 0.00008
Bond angles (°)	0.529 ± 0.004
Ramachandran statistics[c]	
Residues in most favored regions	81.5%
Residues in additional allowed regions	17.9%
Residues in generously allowed regions	0.7%
Residues in disallowed regions	0.0%
Average r.m.s. deviation (Å)[d]	
Heavy atoms (384–508)	1.11 ± 0.14
Backbone atoms (384–508)	0.38 ± 0.11

[a] Hydrogen bonds were identified on the basis of high H^N temperature coefficient (superior to -5×10^{-3} ppm · K^{-1}). Two restraints for each hydrogen bond were included in the calculations ($d_{HN-O} \leq 2.5$Å and $d_{N-O} \leq 3.5$ Å).
[b] The Ca^{2+}-O distances were restrained to 1.8–2.8Å .
[c] Ramachadran statistics were obtained using the PROCHECK NMR software.
[d] CBL1 (411–419) and CBL3 (474–483) were excluded from the r.m.s.d. calculation as they are less well defined.

rounded by two helices, one two-turn α-helix between strands β_6 and β_7 and a one-turn 3^{10}-helix between strands β_7 and β_8 (Fig. 2*B*). As observed in many other C2 domains and also in the Ca^{2+}-free crystal structure of the C2A domain (27), a set of acidic residues is located at one extremity of the protein characterized by three loops (CBL1–3 in Fig. 2*A*). These residues define the CBR.

Ca^{2+} Binding Mode—To determine the Ca^{2+} binding mode of the C2A domain, we first performed a $^1H,^{15}N$ HSQC-based Ca^{2+} titration at pH 5. As expected, the same residues (located in the CBR) observed previously at pH 7 (25) were affected upon Ca^{2+} binding (Fig. 3*A*), indicating that the Ca^{2+} binding mode is topologically not modified at pH 5 as compared with pH 7.

$^1H,^{15}N$ HSQC cross-peaks affected upon Ca^{2+} addition adopted a linear trajectory throughout the titration, allowing the fitting of their chemical shift perturbation against the Ca^{2+} concentration. This also clearly indicates that the C2 domain switches from the unbound state to the fully Ca^{2+}-loaded state without an intermediate state, which means that regardless of the number of Ca^{2+} ions binding to the C2A domain, they bind concomitantly, *i.e.* with very similar affinities. Fitting the chemical shift perturbation of residues affected by Ca^{2+} binding against the Ca^{2+} concentration with Equation 2 to take in account cooperative binding (as suggested by the sigmoidal shape of the curve in Fig. 3*B*) gave a global dissociation constant of 3.76 ± 0.05 mM with a Hill coefficient of 2.27 ± 0.05 (Fig. 3*B*). The lower affinity measured at pH 5 as compared with pH 7 (1.10 ± 0.01 mM) is expected considering the increased protonation state of the acidic residues in the CBR at lower pH. Nevertheless, the pH 5 data are in agreement with those measured at pH 7, *i.e.* the intrinsic Ca^{2+} binding affinity is in the mM range. Noteworthy, the Hill coefficient of 2.27 ± 0.05 measured at pH 5 is identical to the one measured at pH 7 (2.24 ± 0.03). This value indicates that three Ca^{2+} ions should bind in a cooperative way to the C2A domain of rabphilin-3A.

Based on the Ca^{2+} titration and the geometry of the canonical Ca^{2+} binding mode of C2 domains, Ca^{2+} ions were added to the C2A domain structure during the RDC refinement. Only two Ca^{2+} ions were positioned successfully into the canonical sites Ca1 and Ca2 (Fig. 3*C*). Attempting to add a third Ca^{2+} to site Ca3 led to severe RDC and distance restraints violations, in line with mutagenesis results for the C2B domain of synaptotagmin I where the mutation of glycine 368 into a serine residue that is conserved in other C2 domains was a prerequisite to form a third low affinity Ca^{2+} binding site (Fig. 3*C*) (43). Thus, a third Ca^{2+} binding site, indicated by the Hill coefficient of 2.27, may exist in the CBR of the C2A domain. But our NMR data do not allow at present to locate this site.

The Ca^{2+} binding region of the rabphilin-3A C2A domain is shown in Fig. 3*D*. Both Ca^{2+} ions are hexacoordinated, involv-

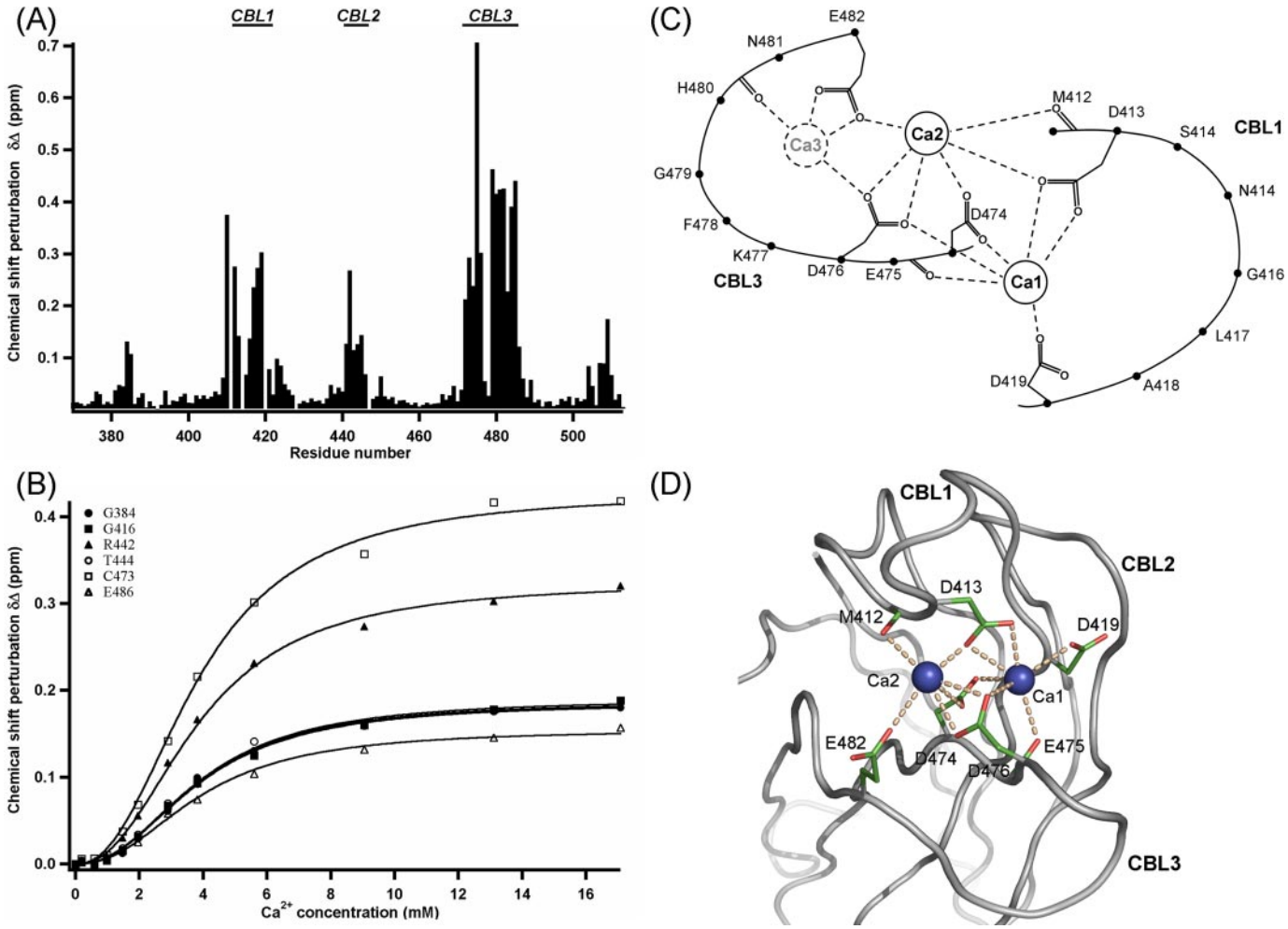

FIGURE 3. **Ca^{2+} binding mode of the rabphilin-3A C2A domain.** *A*, $^{1}H,^{15}N$ chemical shift perturbations δΔ (see "Experimental Procedures") plotted against the sequence of the C2A domain fragment (371–510) upon the addition of 20 mM Ca^{2+}. *B*, simultaneous fit performed on chemical shift perturbations of 6 residue backbone HN cross-peaks according to Ca^{2+} concentration using the Hill equation (Equation 2; see "Experimental Procedures"). *C*, schematic representation of the potential Ca^{2+} binding sites of the C2A domain based on sequence. *Solid circles* represent the two Ca^{2+} binding sites identified by NMR in this study, and the *dotted circle* represents the position of a hypothetical third binding site. *D*, Ca^{2+} binding sites of the C2A domain. The backbone is represented as a *gray ribbon*, *blue spheres* represent the bound Ca^{2+} ions, and residues involved in Ca^{2+} binding are displayed as *green and orange stick models*.

ing four aspartate side chains (Asp-413, -419, -474 and -476), two carbonyl groups (Met-412 and Glu-475), and one glutamate side chain (Glu-482). The involvement of a glutamate side chain has not been observed so far in any structure of a C2 domain.

Structural Comparisons—To compare the Ca^{2+}-free crystal structure with the Ca^{2+}-free conformation in solution, we measured $^{1}D_{^{1}H,^{15}N}$ RDCs on a Ca^{2+}-free sample (in the presence of 5 mM EGTA) aligned in Pf1 bacteriophage at pH 6. Under these conditions most of the CBL resonances are broadened below detection, whereas they are observable in the Ca^{2+}-bound state. Nevertheless, RDC values observed in the core domain were used to determine the alignment tensor using singular value decomposition (44, 45) as implemented in the software PALES (46). The RDCs fit to the Ca^{2+}-free crystal structure with a correlation coefficient of 0.92 and a Q factor of 0.196 (supplemental Fig. 1). These values indicate that in solution, the Ca^{2+}-free form of the C2A domain adopts a conformation very similar to the one observed in the crystal structure.

The Ca^{2+}-free crystal structure and the Ca^{2+}-bound solution structure superpose with an r.m.s.d. value of 0.82 Å for residues 384–509, excluding CBL1 and CBL3 (Fig. 4*A*). Both structures are very similar, indicating that Ca^{2+} binding does not modify the overall structure of the protein. Nevertheless, significant changes are observed within CBL1 and CBL3 (Fig. 4*B*). Both loops adopt very different conformations and positions upon Ca^{2+} binding. Such dramatic changes are in agreement with the finding that in the Ca^{2+}-free crystal structure the conformations and positions of the acidic side chains of the prospective Ca^{2+} binding residues within these loops are not compatible with Ca^{2+} binding.

In the Ca^{2+}-bound structure, CBL1 adopts an open conformation by digressing from CBL3. More specifically, the conformation of Asp-413 changes in order to chelate Ca^{2+} in position Ca1. Residues Asp-419 and -476 also chelate this ion, but these two residues already adopt a rather favorable conformation in the Ca^{2+}-free crystal structure. As mentioned above, the Ca^{2+}-induced conformational change of residue Asp-413 seems also to go along with a large rearrangement of most of the CBL1 residues (Fig. 4*B*). In addition, CBL3 bends toward the tip of the domain, leaving the basic concave side more exposed to solvent. Moreover, Ca^{2+} binding induces important conformational

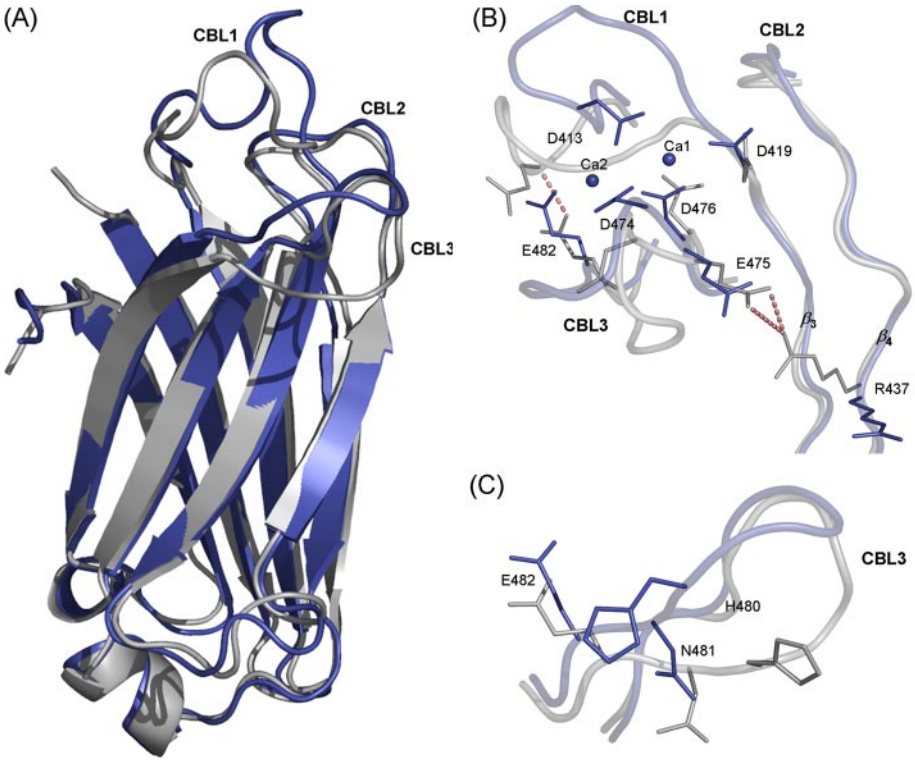

FIGURE 4. **Structure comparison of the Ca^{2+}-bound form and Ca^{2+}-free form of the rabphilin-3A C2A domain.** *A*, backbone superposition of the Ca^{2+}-bound solution structure of the C2A domain (in *blue*) with the Ca^{2+}-free crystal structure (in *gray*). *B*, Ca^{2+} binding site comparison of the Ca^{2+}-bound form (in *blue*) with the Ca^{2+}-free form (in *gray*). Backbones are represented by *ribbons*, side chains of residues involved in Ca^{2+} binding are represented by *sticks*, and Ca^{2+} ions are depicted as *blue spheres*. *C*, comparison of the CBL3 conformation in the Ca^{2+}-bound (*blue*) and Ca^{2+}-free (gray) form of the C2A domain.

changes for residues Asp-474 and Glu-482 (Fig. 4*B*). In particular, two hydrogen bonds observed in the Ca^{2+}-free crystal structure are not present anymore in the Ca^{2+}-bound form, one between the side chain of residue Glu-482 and the amide group of residue Asp-413, the other one between the carboxylic group of Glu-475 (from the DED motif located in CBL3) and the guanidinium group of Arg-437 (from strand β_3). This last observation is also confirmed by the fact that β and γ protons of Glu-475 exhibit chemical shift degeneracy, revealing a high flexibility of the Glu-475 side chain. Noteworthy, conformations of residues throughout CBL3 also change significantly, including the basic residues His-480 and Asn-481 involved in PIP2 headgroup binding (see below) (Fig. 4*C*).

IP3 Binding to the C2A Domain—As shown above, Ca^{2+} binding to the C2 domain of rabphilin-3A induces large conformational changes in CBL1 and CBL3. These changes might play an important role in the Ca^{2+}-dependent IP3 binding to the C2A domain. Therefore, we probed the IP3 binding properties of this C2 domain by performing a $^1H,^{15}N$ HSQC-based titration at pH 5 and in presence of 20 mM Ca^{2+}. Large chemical shift perturbations were observed for a limited set of residues located on the concave side of the core domain, namely on the strands β_3 and β_4, and on CBL3, forming a polybasic stretch (Fig. 5*A*). The saturation was not reached at 3 mM IP3. Nevertheless, a reasonable simultaneous fit with Equation 1 using chemical shift perturbations from 16 HN cross-peaks could be performed and gave a K_D value of 1.30 ± 0.03 mM (Fig. 5*B*). This much lower affinity compared with the value measured at pH 7 (55 μM) (25) can be explained by the increased protonation state of the IP3 phosphate groups, loosening the interaction with the polybasic stretch of the C2A domain. Nevertheless, the chemical shift perturbation pattern perfectly overlaps with the one observed at pH 7 (data not shown), indicating that the IP3 binding mode at pH 5 does not differ from pH 7. However, most resonances of residues located in CBL3 are broadened out at pH 7, which makes the accurate evaluation of their involvement in IP3 binding difficult. At pH 5, these resonances are clearly observable, allowing the investigation of their involvement in IP3 binding. Indeed, as shown in Fig. 5*C*, most of CBL3 constitutes the third region of the IP3 binding site in addition to the strands β_3 and β_4. Moreover, the large amplitude of chemical shift deviations of cross-peaks of residues in CBL3 (Fig. 5*A*), compared with those of both β strands, suggests the active involvement of this Ca^{2+} binding loop in IP3 binding.

Resonances of the basic residues His-480 and Asn-481 are the most perturbed resonances of CBL3 upon IP3 titration. To probe the role of these basic residues in IP3 binding, two single point mutants have been designed: H480A and N481A. These two mutants were ^{15}N-labeled, and $^1H,^{15}N$ HSQC-based IP3 titrations were performed at pH 7 in the presence of 20 mM Ca^{2+} to determine affinity values at more physiological conditions. K_D values were obtained from a simultaneous fitting procedure. The H480A and N481A mutants showed significantly higher K_D values of 360 ± 10 and 930 ± 30 μM, respectively (supplemental Fig. 2) as compared with the wild type protein (55 μM). Meanwhile the intrinsic Ca^{2+} binding affinities of these mutants were only slightly affected. The K_D was 1.46 mM for H480A and 1.1 mM for N481A compared with a K_D of 1.1 mM for the wild type C2A domain (data not shown). The strong decreases in IP3 affinity clearly indicate the active involvement of His-480 and Asn-481 in IP3 binding. Thus, residues from CBL3 define in addition to the polybasic stretch the PIP2 headgroup binding site of the C2A domain of rabphilin-3A.

IP3-C2A Domain Docking Models—The $^1H,^{15}N$ HSQC-based IP3 titration performed at pH 5 and the data available for the H480A and N481A mutants provide a very well defined view of the IP3 binding mode to the C2A domain of rabphilin-3A. To derive a model of the IP3-C2A complex, we used these experimental data in a docking approach. The docking procedure was driven with HADDOCK 2.0, using the five lowest energy structures of the Ca^{2+}-bound rabphilin-3A C2A

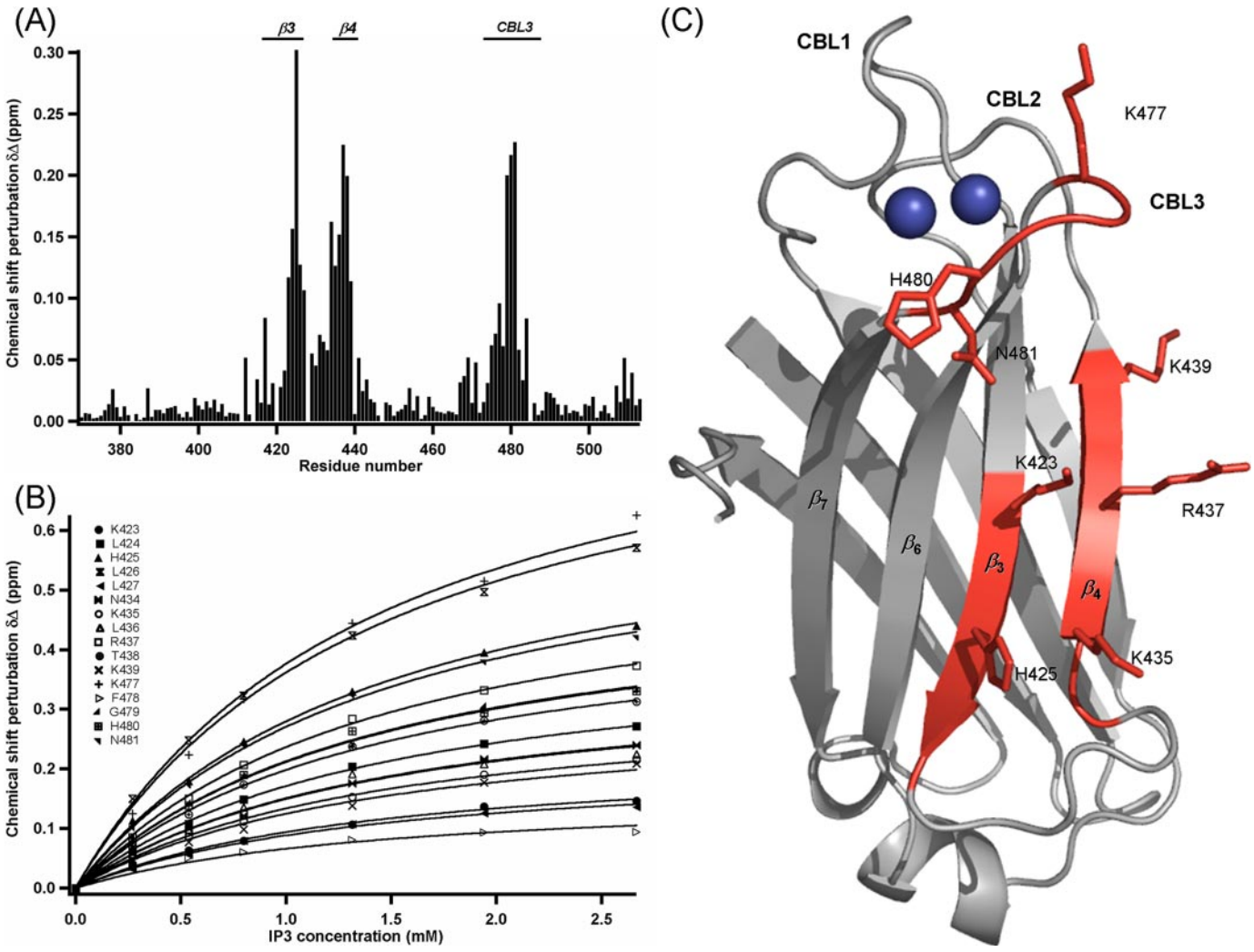

FIGURE 5. **IP3 binding mode of the rabphilin-3A C2A domain at pH 5.** *A*, $^{1}H,^{15}N$ chemical shift perturbations δΔ (see "Experimental Procedures") plotted against the sequence of the C2A domain fragment (371–510) upon the addition 3 mM IP3 at pH 5 in presence of 20 mM Ca^{2+}. *B*, simultaneous fit performed on chemical shift perturbations of 16 residue backbone HN cross-peaks according to IP3 concentration using Equation 1 (see "Experimental Procedures"). *C*, mapping on the solution structure of the C2A domain of residues whose $^{1}H,^{15}N$ cross-peaks experienced significant chemical shift perturbations in presence of 3 mM IP3 (colored in *red*). Side chains of basic residues belonging to the affected parts of the protein are also shown (represented as *sticks*), and Ca^{2+} ions are represented as *blue spheres*.

domain as starting coordinates. PIP2 (1,2-diacetoyl-*sn*-3-[phosphoinositol-3,4,5-trisphosphate]) was docked to mimic a polar head from a lipid embedded in the plasma membrane. ambiguous interaction restraints were defined between the protein and the IP3 moiety of PIP2 to match the experimental conditions, where IP3 was used in the titrations. The docking protocol used led to an ensemble of 50 structures after water refinement. The 50 structures were ranked according to their HADDOCK score (Table 2). A single cluster of solutions was found within the final ensemble, and the three best models were selected as the final representative ensemble of the complex structure. Statistical data for the final ensemble are summarized in Table 2. Ligand position and orientation are well conserved (Fig. 6*A*), in line with the low r.m.s.d. value measured at the protein/ligand interface of 1.32 ± 0.59 Å.

As shown in Fig. 6*B*, the PIP2 molecule binds to the concave side of the domain and interacts with basic residues from CBL3 and strands β_3 and β_4. The residue His-425 interacts with phosphate 4, residues Lys-435 and Arg-437 interact with phosphate 3, and residues Lys-423, His-480, and Asn-481 interact with phosphate 1 of PIP2. In particular, the His-480–Asn-481 pair acts as a clamp fixing phosphate 1. Because of these interactions, the PIP2 molecule lies flat on the concave surface of the β-sheet, with the diacetoylglycerol chain pointing toward the CBR (Fig. 6*B*).

Comparison of the C2A domain conformation in its IP3-free and IP3-bound forms suggests that PIP2 binding does not require major protein backbone conformational changes (backbone r.m.s.d. of 0.67 Å between the two forms). Even the CBL3, which was defined as a fully flexible segment during the calculations, exhibits only slightly different conformations, indicating that the Ca^{2+}-bound form of the C2A domain adopts a conformation adjusted for the interaction with IP3. Overall, the Ca^{2+}/IP3-bound C2A domain structure is much closer to its Ca^{2+}-bound structure than to its Ca^{2+}-free structure, revealing structural features underlying Ca^{2+} dependence of IP3 binding.

Ca^{2+}/IP3 Binding Cooperativity—Ca^{2+} binding to the C2A domain triggers IP3 binding. Moreover, Ca^{2+} loading of the

TABLE 2
Docking parameters and statistics

Runs	Protocol	Docking protocol					
		Steps	T (K)	Space[a]	Backbone	Side chains	Ligand
1000	Minimization				Rigid	Rigid	Rigid
300	MD	500	2000	TA	Rigid	Rigid	Rigid
300	SA	500	2000 → 50	TA	Rigid	Rigid	Rigid
300	SA	2000	1000 → 50	TA	Rigid	Flexible	Flexible
300	SA	2000	1000 → 50	TA	Flexible	Flexible	Flexible
50	Water refinement			CA	Flexible	Flexible	Flexible
Docking parameters							
Active residues				423, 425, 435, 437, 480, 481			
Semi-flexible residues				423, 425, 435, 437, 480, 481			
Fully flexible segment				476–481			
Structural statistics							
Backbone r.m.s.d. (Å) with respect to the mean							
Interface protein				2.01 ± 0.36			
Interface ligand				1.86 ± 0.69			
Interface all				1.90 ± 0.62			
Intermolecular energies after water refinement							
E_{tot} (kcal · mol^{-1})				−5748 ± 76			
E_{VdW} (kcal · mol^{-1})				−523 ± 8			
E_{elec} (kcal · mol^{-1})				−6159 ± 73			
E_{AIR} (kcal · mol^{-1})				0.01 ± 0.007			
Edesolv (kcal · mol^{-1})				1.68 ± 0.87			
HADDOCK score (kcal · mol^{-1})[b]				−1753 ± 10			

[a] TA, torsion angle space; CA, cartesian space.
[b] Defined as the weighted sum of different terms ($1\times E_{VDW} + 0.2E_{elec} + 0.1E_{AIR} + 1 \times E_{desolv}$).

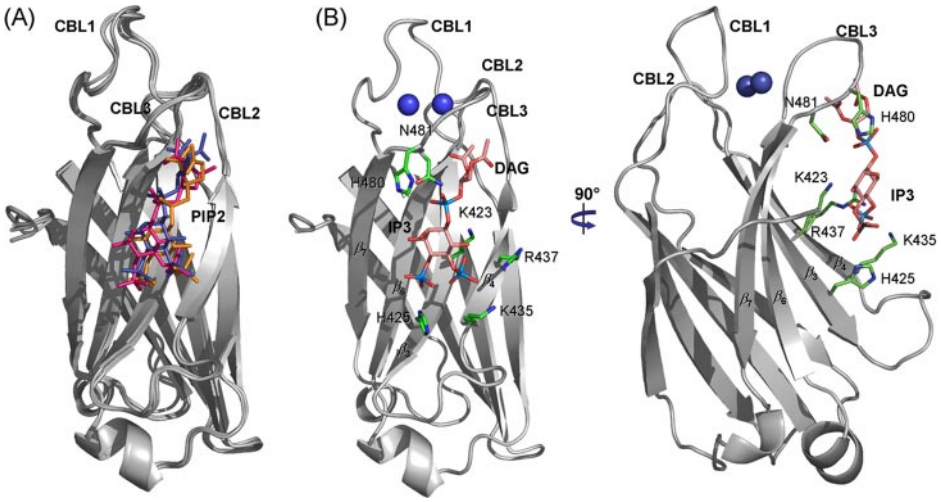

FIGURE 6. **Docking models of the PIP2-rabphilin-3A C2A domain complex.** *A*, ribbon representation of the final ensemble of models for the C2A-PIP2 complex, and PIP2 is represented in *sticks* and various colors. *B*, ribbon representations of the most representative model of the C2A-PIP2 complex. Side chains of residues probably actively involved in the binding are represented in *sticks* and colored in *green*, the PIP2 molecule is depicted in various colors, and Ca^{2+} ions are shown as *blue spheres*.

C2A domain is greatly increased in the presence of IP3 (25). This phenomenon is known as target-activated messenger affinity mechanism, recently defined by Corbin *et al.* (26). It is reasonable to assume that IP3 binding will promote a similar conformational change on the CBR as the one induced by Ca^{2+} and subsequently enhance Ca^{2+} binding to the C2A domain.

The very low affinity of the Ca^{2+}-free form for IP3 (0.8 mM) hinders NMR structural studies with conventional methods such as the measurement of RDCs or intermolecular NOEs. As an alternative approach to address this question we designed two mutants of the C2A domain with the aim to mimic, directly or indirectly, IP3 saturation.

The R437A mutant was designed based on our recent observation that Glu-475 from the DED motif on CBL3 interacts with Arg-437 from strand β_4 via a hydrogen-bond network between the carboxylic group of Glu-475 and the guanidinium group of Arg-437 in the Ca^{2+}-free crystal structure (27). In the Ca^{2+}-bound solution structure, this interaction does not exist anymore (Fig. 4*B*). Moreover, the β and γ protons of Glu-475 exhibit chemical shift degeneracy, revealing a high flexibility of the Glu-475 side chain. This implies that Ca^{2+} binding breaks the interaction between Glu-475 and Arg-437, releasing the Arg-437 side chain, thus allowing a stronger interaction of Arg-437 with IP3, as shown by our docking model.

The N481D mutant was designed to mimic the presence of a phosphate group on the concave side of the core domain (namely the IP3 binding site). Our working hypothesis was that the Asp-481 side chain should interact with the basic residues of the concave side, shifting CBL3 into a conformation similar to the one observed in the IP3-C2A docking model.

Both mutants, R437A and N481D, were ^{15}N-labeled, and ^{1}H,^{15}N HSQC-based Ca^{2+} titrations were performed at pH 7. K_D values were obtained from a simultaneous fitting procedure using Equation 2 (see "Experimental Procedures"). Both mutants showed significantly lower K_D values of 477 ± 7 and 305 ± 4 μM, respectively (supplemental Fig. 3), as compared with the wild type C2A domain (1.1 mM). Moreover, both mutants exhibited lower cooperativity than the wild type domain with Hill coefficients of 1.62 ± 0.01 and 1.63 ± 0.01 for

R437A and the N481D, respectively. Thus, both mutations facilitate Ca^{2+} binding. The affinity of these mutants for IP3 was also measured in presence of saturating concentration of Ca^{2+}. For both mutants the saturation was not reached at 3 mM IP3. The R437A mutant exhibits a much higher K_D value of 673 ± 36 μM as compared with the wild type protein (55 μM) (supplemental Fig. 4). For the N481D mutant, the IP3 binding to the concave side almost vanished; only very weak chemical shift perturbations were observed at 3 mM IP3.

The Arg-437 and Asn-481 mutant data clearly demonstrate that not only residues from the basic patch but also residues on CBL3 constitute the structural link between Ca^{2+} and PIP2 binding to the C2A domain of rabphilin-3A. This points out the functional importance of the conformational change of CBL3 for PIP2 binding as predicted from our docking model.

DISCUSSION

The aim of this work was to gain further insight of the interplay between the C2A domain of rabphilin-3A, Ca^{2+}, and PIP2 binding at the atomic level. To achieve this goal, the NMR structure of the Ca^{2+}-bound C2A domain was required because only the Ca^{2+}-free crystal structure of this domain had been described so far (27). Because of the low Ca^{2+} binding affinity of the isolated C2A domain in solution (320 μM in presence and 1.1 mM in absence of IP3 at pH 7 (25)), its Ca^{2+}-bound NMR structure had to be determined at an apparently unphysiologically high Ca^{2+} concentration (20 mM). This low intrinsic Ca^{2+} binding affinity is well known for C2 domains. It turns into a high apparent Ca^{2+} binding affinity in the presence of the target phospholipids, which complete the Ca^{2+} coordination spheres. The gain between the low intrinsic Ca^{2+} binding affinity in the absence of phospholipids and the high apparent Ca^{2+} binding affinity of C2 domains in their presence can reach up to 3 orders of magnitude (47). In the case of rabphilin-3A, the C2B domain should actually dock to the membrane first (25) due to its much higher intrinsic Ca^{2+} binding affinity (28) compared with the C2A domain, resulting in a high local concentration of phosphatidylserine, the primary lipid target of the C2 domains of rabphilin-3A, and thus, in a dramatic decrease of the K_d of the C2A domain for Ca^{2+} binding. Synergistically, an increase of the Ca^{2+} binding affinity upon Ca^{2+}-dependent binding of the C2A domain to PIP2 may then further strengthen the interaction between the C2A domain and the membrane at physiological Ca^{2+} concentrations, in line with our Ca^{2+} titration data in the presence of IP3 (25).

In this context the question arises if IP3 is a good mimic at all to study the interaction of PIP2 with the Ca^{2+}-loaded C2A domain. As already mentioned above, phosphatidylserine was identified as the key phospholipid enabling high apparent Ca^{2+} binding affinity for the C2 domains of rabphilin-3A via the Ca^{2+} bridging mechanism, whereas PIP2 was shown to further increase the membrane binding affinity by specific Ca^{2+}-dependent interaction with both C2 domains (14). Here we have confirmed that in solution IP3 interacts indeed in a specific Ca^{2+}-dependent manner with the C2A domain. We were able to delineate the molecular determinants of this interaction that increases the intrinsic Ca^{2+} binding affinity of this domain but differs from the Ca^{2+} bridging mechanism. This is in agreement with the higher membrane binding affinity of the C2A domain in the presence of PIP2 observed in liposome binding experiments (14). Moreover, the Ca^{2+} binding affinity resulting from IP3 binding to the C2A domain is comparable with the Ca^{2+} binding affinities observed for the C2 domains of synaptotagmin I in solution (48). Noteworthy, the Ca^{2+} binding affinity determined here is close to the concentrations of Ca^{2+} microdomains required for the vesicle fusion process (49). For several other C2 domains it was also shown that the formation of localized pools of PIP2 plays an important role for enhancing Ca^{2+} binding affinity (26, 50). This may also be the case for the C2 domains of rabphilin-3A.

It is widely assumed that Ca^{2+} binding to C2 domains does not induce major conformational changes and that the interaction with acidic phospholipids takes place by the change of the electrostatic potential of the CBR upon Ca^{2+} binding (47). Here we have shown that the C2A domain of rabphilin-3A does not follow this rule. Indeed, structural comparison of the Ca^{2+}-bound form with the Ca^{2+}-free form revealed that Ca^{2+} binding induces large conformational changes within CBL1 and CBL3 and leads to the rupture of two hydrogen bonds (between Glu-482 and Asp-413 and between Glu-475 and Arg-437 (Fig. 4*B*)). These conformational changes are probably associated with a high activation energy, which explains the low affinity of the C2A domain for Ca^{2+} and the strong, structurally determined cooperativity between the two Ca^{2+} binding sites. Very similar properties were also observed for EF-hand Ca^{2+} binding modules found *e.g.* in calmodulin or calbindin where the transition from the Ca^{2+}-free to the Ca^{2+}-bound form involves major conformational rearrangements (51).

Next, comparison of the Ca^{2+}-bound structure with the Ca^{2+}-free form (27) reveals that the Ca^{2+}-induced conformational change of the CBR appears to trigger the interaction with IP3 by shifting the CBL3 into a favorable conformation. Indeed, the NMR structure of the Ca^{2+}-bound C2A domain shows a conformational change in the CBR (Fig. 4), resulting in a larger exposure of the concave side of the C2 domain, which harbors the basic cluster essential for PIP2 binding to C2 domains (52). Moreover, our mutagenesis studies and our docking model show that residues His-480 and Asn-481 from CBL3 also play a central role in IP3 binding by clamping the phosphate 1 of IP3, whereas the other phosphates interact with basic residues from the strands β_3 and β_4 of the core domain (Fig. 6). In particular, Asn-481 is clearly essential for IP3 binding as its mutation into alanine led to the most pronounced decrease in affinity (930 ± 30 μM) as compared with H480A (360 ± 10 μM) and R437A (673 ± 36 μM). Notably, Asn-481 is well conserved in PIP2 binding C2 domains (Fig. 1).

Previously, only the basic patch located on the concave side of the domain has been described as IP3 recognition site (8). Here, we have shown that, in addition, residues from CBL3 are essential for IP3 recognition. Moreover, as CBL3 is involved in Ca^{2+} binding, these residues very likely couple IP3 and Ca^{2+} binding. Indeed, Ca^{2+} binding to the C2A domain facilitates IP3 binding via a conformational change of the CBR, particularly within CBL3. On the contrary, in the Ca^{2+}-free form CBL3 has to undergo a large conformational change to promote IP3 binding. This energetically unfavorable rearrangement is in

good agreement with the very low IP3 affinity observed for the Ca^{2+}-free form of the C2A domain (25). It is also consistent with the fact that Ca^{2+} loading of the C2A domain is greatly increased by the presence of IP3 in a target-activated messenger affinity mechanism. Indeed, if the binding of IP3 provokes a conformational change of CBL3, the energetic cost of activation for Ca^{2+} binding should be reduced, which is supported by our mutagenesis studies showing that directly (N481D) or indirectly (R437A) induced conformational changes of CBL3 facilitate Ca^{2+} binding.

The docking model presented in this work is based on the Ca^{2+}-bound C2A solution structure. It differs from our previous, Ca^{2+}-free crystal structure-based model by including the direct interaction of His-480 and Asn-481 with the PIP2 headgroup. This docking model takes into account the structural changes in CBL3 upon Ca^{2+} binding and the direct involvement of CBL3 in PIP2 binding as shown by our extensive chemical shift mapping of IP3 binding at pH 5.0 as well as by the IP3 binding of several mutants at pH 7.0. The resulting positioning of PIP2 parallel to the main axis of the C2A domain implies that the C2A domain must be sitting rather flat on the membrane surface to keep the phosphate 1 group of PIP2 as well as the Ca^{2+} ions in the phosphate layer of the membrane (53). The perpendicular orientation of the inositol ring to the main axis of the C2A domain in our previous model (25) was also in line with a flat positioning of the C2A domain on the membrane. But in the light of the data for the Ca^{2+}-bound C2A domain presented here this former docking model lacked the interaction with CBL3 residues as an essential feature for a detailed structural and functional description of the Ca^{2+}-dependent C2A domain-PIP2 interaction.

We were able to explain in this work the remarkable interconnection of the Ca^{2+} and PIP2 binding of the C2A domain of rabphilin-3A. This was possible because of the availability of the structures in Ca^{2+}-free and Ca^{2+}-bound form combined with the full description of the IP3 binding site on the C2A domain. Taken together, our results show how the interdependency of Ca^{2+} and IP3 binding is mediated by CBL3. As a functional consequence, this structural feature implies that both the messenger (Ca^{2+}) and the target (PIP2) have to be simultaneously present to trigger an efficient targeting of the C2A domain to the plasma membrane. It would be highly interesting to find out if the structural determinants that we found for the interdependency of PIP2 and Ca^{2+} binding in this C2A domain are unique or if this architecture is used more generally in C2 domains with similar functional features.

Acknowledgments—We thank Ann-Kathrin Brückner for technical help and Christian Griesinger for useful discussions and generous support.

REFERENCES

1. Nishizuka, Y. (1988) *Nature* **334,** 661–665
2. Nalefski, E. A., and Falke, J. J. (1996) *Protein Sci.* **5,** 2375–2390
3. Verdaguer, N., Corbalan-Garcia, S., Ochoa, W. F., Fita, I., and Gomez-Fernandez, J. C. (1999) *EMBO J.* **18,** 6329–6338
4. Nalefski, E. A., and Falke, J. J. (1998) *Biochemistry* **37,** 17642–17650
5. Ananthanarayanan, B., Das, S., Rhee, S. G., Murray, D., and Cho, W. (2002) *J. Biol. Chem.* **277,** 3568–3575
6. Tucker, W. C., Edwardson, J. M., Bai, J., Kim, H. J., Martin, T. F., and Chapman, E. R. (2003) *J. Cell Biol.* **162,** 199–209
7. Bolsover, S. R., Gomez-Fernandez, J. C., and Corbalan-Garcia, S. (2003) *J. Biol. Chem.* **278,** 10282–10290
8. Cho, W., and Stahelin, R. V. (2006) *Biochim. Biophys. Acta* **1761,** 838–849
9. Golub, T., and Caroni, P. (2005) *J. Cell Biol.* **169,** 151–165
10. Osborne, S. L., Wen, P. J., and Meunier, F. A. (2006) *J. Neurochem.* **98,** 336–342
11. Evans, J. H., Murray, D., Leslie, C. C., and Falke, J. J. (2006) *Mol. Biol. Cell* **17,** 56–66
12. Rodriguez-Alfaro, J. A., Gomez-Fernandez, J. C., and Corbalan-Garcia, S. (2004) *J. Mol. Biol.* **335,** 1117–1129
13. Grishanin, R. N., Kowalchyk, J. A., Klenchin, V. A., Ann, K., Earles, C. A., Chapman, E. R., Gerona, R. R., and Martin, T. F. (2004) *Neuron* **43,** 551–562
14. Chung, S. H., Song, W. J., Kim, K., Bednarski, J. J., Chen, J., Prestwich, G. D., and Holz, R. W. (1998) *J. Biol. Chem.* **273,** 10240–10248
15. Schiavo, G., Gu, Q. M., Prestwich, G. D., Sollner, T. H., and Rothman, J. E. (1996) *Proc. Natl. Acad. Sci. U. S. A.* **93,** 13327–13332
16. Haucke, V. (2005) *Biochem. Soc. Trans.* **33,** 1285–1289
17. Cremona, O., and De Camilli, P. (2001) *J. Cell Sci.* **114,** 1041–1052
18. Shirataki, H., Kaibuchi, K., Sakoda, T., Kishida, S., Yamaguchi, T., Wada, K., Miyazaki, M., and Takai, Y. (1993) *Mol. Cell. Biol.* **13,** 2061–2068
19. Miyazaki, M., Shirataki, H., Kohno, H., Kaibuchi, K., Tsugita, A., and Takai, Y. (1994) *Biochem. Biophys. Res. Commun.* **205,** 460–466
20. Zhang, Y., Luan, Z., Liu, A., and Hu, G. (2001) *FEBS Lett.* **497,** 99–102
21. Willshaw, A., Grant, K., Yan, J., Rockliffe, N., Ambavarapu, S., Burdyga, G., Varro, A., Fukuoka, S., and Gawler, D. (2004) *FEBS Lett.* **559,** 13–21
22. Tsuboi, T., and Fukuda, M. (2005) *J. Biol. Chem.* **280,** 39253–39259
23. Deak, F., Shin, O. H., Tang, J., Hanson, P., Ubach, J., Jahn, R., Rizo, J., Kavalali, E. T., and Sudhof, T. C. (2006) *EMBO J.* **25,** 2856–2866
24. McKiernan, C. J., Stabila, P. F., and Macara, I. G. (1996) *Mol. Cell. Biol.* **16,** 4985–4995
25. Montaville, P., Coudevylle, N., Radhakrishnan, A., Leonov, A., Zweckstetter, M., and Becker, S. (2008) *Protein Sci.* **17,** 1025–1034
26. Corbin, J. A., Evans, J. H., Landgraf, K. E., and Falke, J. J. (2007) *Biochemistry* **46,** 4322–4336
27. Biadene, M., Montaville, P., Sheldrick, G. M., and Becker, S. (2006) *Acta Crystallogr. D Biol. Crystallogr.* **62,** 793–799
28. Montaville, P., Schlicker, C., Leonov, A., Zweckstetter, M., Sheldrick, G. M., and Becker, S. (2007) *J. Biol. Chem.* **282,** 5015–5025
29. Delaglio, F., Grzesiek, S., Vuister, G. W., Zhu, G., Pfeifer, J., and Bax, A. (1995) *J. Biomol. NMR* **6,** 277–293
30. Bartels, C., Xia, T. H., Billeter, M., Guntert, P., and Wuthrich, K. (1995) *J. Biomol. NMR* **6,** 1–10
31. Keller, R. (2004) *The Computer-aided Resonance Assignment Tutorial*, Cantina Verlag, Goldau, Switzerland
32. Montaville, P., Kim, H. Y., Vijayan, V., Becker, S., and Zweckstetter, M. (2006) *J Biomol NMR* **36,** Suppl. 1, 20
33. Ottiger, M., and Bax, A. (1998) *J. Biomol. NMR* **12,** 361–372
34. Cornilescu, G., Delaglio, F., and Bax, A. (1999) *J. Biomol. NMR* **13,** 289–302
35. Herrmann, T., Guntert, P., and Wuthrich, K. (2002) *J. Biomol. NMR* **24,** 171–189
36. Herrmann, T., Guntert, P., and Wuthrich, K. (2002) *J. Mol. Biol.* **319,** 209–227
37. Güntert, P. (2003) *Prog. Nucl. Magn. Reson. Spectrosc.* **43,** 105–125
38. Baxter, N. J., and Williamson, M. P. (1997) *J. Biomol. NMR* **9,** 359–369
39. Schwieters, C. D., Kuszewski, J. J., Tjandra, N., and Clore, G. M. (2003) *J. Magn. Reson.* **160,** 65–73
40. Auguin, D., Barthe, P., Royer, C., Stern, M. H., Noguchi, M., Arold, S. T., and Roumestand, C. (2004) *J. Biol. Chem.* **279,** 35890–35902
41. Dominguez, C., Boelens, R., and Bonvin, A. M. (2003) *J. Am. Chem. Soc.* **125,** 1731–1737
42. Brunger, A. T., Adams, P. D., Clore, G. M., DeLano, W. L., Gros, P., Grosse-Kunstleve, R. W., Jiang, J. S., Kuszewski, J., Nilges, M., Pannu, N. S., Read, R. J., Rice, L. M., Simonson, T., and Warren, G. L. (1998) *Acta*

Crystallogr. D Biol. Crystallogr. **54,** 905–921
43. Fernandez, I., Arac, D., Ubach, J., Gerber, S. H., Shin, O., Gao, Y., Anderson, R. G., Sudhof, T. C., and Rizo, J. (2001) *Neuron* **32,** 1057–1069
44. Losonczi, J. A., Andrec, M., Fischer, M. W., and Prestegard, J. H. (1999) *J. Magn. Reson.* **138,** 334–342
45. Selvan, S., and Ramakrishnan, S. (2007) *IEEE Trans. Image Process.* **16,** 2688–2696
46. Zweckstetter, M. (2008) *Nat. Protoc.* **3,** 679–690
47. Rizo, J., and Sudhof, T. C. (1998) *J. Biol. Chem.* **273,** 15879–15882
48. Ubach, J., Lao, Y., Fernandez, I., Arac, D., Sudhof, T. C., and Rizo, J. (2001) *Biochemistry* **40,** 5854–5860
49. Neher, E. (1998) *Neuron* **20,** 389–399
50. Landgraf, K. E., Malmberg, N. J., and Falke, J. J. (2008) *Biochemistry* **47,** 8301–8316
51. Gifford, J. L., Walsh, M. P., and Vogel, H. J. (2007) *Biochem. J.* **405,** 199–221
52. Corbalan-Garcia, S., Garcia-Garcia, J., Rodriguez-Alfaro, J. A., and Gomez-Fernandez, J. C. (2003) *J. Biol. Chem.* **278,** 4972–4980
53. Rufener, E., Frazier, A. A., Wieser, C. M., Hinderliter, A., and Cafiso, D. S. (2005) *Biochemistry* **44,** 18–28